Saudi Journal of Biological Sciences (2017) 24, 451–458

King Saud University

Saudi Journal of Biological Sciences

www.ksu.edu.sa
www.sciencedirect.com

ORIGINAL ARTICLE

Efficient purification protocol for bioengineering allophycocyanin trimer with N-terminus Histag

Wenjun Li [a,c,1], Yang Pu [b,1], Na Gao [d], Zhihong Tang [a], Lufei Song [a], Song Qin [a,*]

[a] Yantai Institute of Coastal Zone Research, Chinese Academy of Sciences, Yantai 264003, China
[b] School of Agriculture, Ludong University, Yantai 264025, China
[c] University of Chinese Academy of Sciences, Beijing 100049, China
[d] South China Sea Institute of Oceanology, Chinese Academy of Sciences, Guangzhou 510301, China

Received 7 December 2016; revised 30 December 2016; accepted 6 January 2017
Available online 21 January 2017

KEYWORDS

Efficient purification;
Bioengineering allophycocyanin trimer;
Optimization;
Histag

Abstract Allophycocyanin plays a key role for the photon energy transfer from the phycobilisome to reaction center chlorophylls with high efficiency in cyanobacteria. Previously, the high soluble self-assembled bioengineering allophycocyanin trimer with N-terminus polyhistidine from *Synechocystis* sp. PCC 6803 had been successfully recombined and expressed in *Escherichia coli* strain. The standard protocol with immobilized metal-ion affinity chromatography with chelating transition metal ion (Ni^{2+}) was used to purify the recombinant protein. Extensive optimization works were performed to obtain the desired protocol for high efficiency, low disassociation, simplicity and fitting for large-scale purification. In this study, a 3^3 full factorial response surface methodology was employed to optimize the varied factors such as pH of potassium phosphate (X_1), NaCl concentration (X_2), and imidazole concentration (X_3). A maximum trimerization ratio (Y_1) of approximate $A_{650\ nm}/A_{620\ nm}$ at 1.024 was obtained at these optimum parameters. Further examinations, with absorbance spectra, fluorescence spectra and SDS-PAGE, confirmed the presence of bioengineering allophycocyanin trimer with highly trimeric form. All these results demonstrate that optimized protocol is efficient in purification of bioengineering allophycocyanin trimer with Histag.

1. Introduction

Nature has been developing and optimizing photosynthesis for billions years. Phycobilisomes, which are the main light harvesting complexes in cyanobacteria and red algae, absorb and transfer solar energy to photosynthetic reaction center with capability of broad range visible spectrum and high efficiency (Lowe, 2007; Nelson and Yocum, 2006; Adir, 2005; Adir et al., 2007). Allophycocyanin (APC) trimer is the primary composition of phycobilisomes core, containing only phycocyanobilin (PCB), for efficient lower-energy photons

* Corresponding author at: Yantai Institute of Coastal Zone Research, Chinese Academy of Sciences, Yantai 264003, China.
E-mail address: cpra_yic@sina.com (S. Qin).
[1] Wenjun Li and Yang Pu are co-first authors.
Peer review under responsibility of King Saud University.

Production and hosting by Elsevier

http://dx.doi.org/10.1016/j.sjbs.2017.01.011

funneling pathway. Moreover, it is also the basic unit to finish bio-functions in photosynthesis in cyanobacteria and red algae (MacColl, 2004; MacColl et al., 2003). APC trimers $(\alpha\beta)_3$ are self-assembled by three monomers ($\alpha\beta$) which were initiated with the docking process of α and β subunits (Adir, 2005; Adir et al., 2007). Recently, the relatively high-resolution images with X-ray crystallography and electron microscopy have revealed the details of native APC trimer structures from cyanobacteria (McGregor et al., 2008; Arteni et al., 2009). The direct structural proof of the APC trimer from *Synechocystis* sp. PCC 6803 by electron microscopy revealed a flattened disk structure with proximately 3 nm in short axis, 12 nm in long axis and a central hole of 3 nm in diameter (MacColl, 2004; Arteni et al., 2009). Recent study showed that the photon energy transfer in APC trimer from the core into reaction center chlorophylls may follow the mechanism of Förster resonance on a time scale 430–440 femtoseconds with unbelievable efficiency (MacColl, 2004). Moreover, APC trimer was wide used as fluorescent tags, antioxidant and anti-enterovirus, except for the bio-functions in photosynthesis (Su et al., 2010; Liu et al., 2010). However, in cyanobacteria, APC is a minor constituent in three types of phycobiliproteins, compared with phycocyanin (PC) and phycoerythrin (PE) (Su et al., 2010; Bermejo et al., 1997). Thus, the difficulty of purification of APC trimer with high efficiency is a current major inhibitor of its applications.

For this reason, in 2009, Liu et al. reported highly soluble self-assembled bioengineering allophycocyanin (bAPC) trimer with N-terminus polyhistidine (14 unstructured residues including 6 × Histag) from *Synechocystis* sp. PCC 6803 for the first time, which were expressed in *Escherichia coli* strain. For the construction of engineering strain, two constructed expression vectors were co-transformed into *E. coli* with an entire biosynthesis pathway of bAPC trimer (Liu et al., 2010; Tooley et al., 2001). Specifically, the full-length gene of apoprotein α subunit (*apcA*) was cloned into one cassette in the pCDFDeut-1 expression vector and the full-length genes of heme oxygenase 1 (*hox1*) and 3z-phycocyanobilin ferredoxin oxidoreductase (*pcyA*) were cloned into another cassette in the same expression vector; the full-length gene of apoprotein β subunit (*apcB*) was cloned into one cassette in the pRSFDeut-1 expression vector and the full-length genes of heterodimeric lyases (*cpcS-1* and *cpcU*) were cloned into another cassette in the same expression vector. Native structure, stability and fluorescent characteristics of the bAPC trimer have been demonstrated by fluorescence and absorption spectrometry analyses, supporting previous reports (Liu et al., 2010). In addition, the presence of N-terminus which extends out from the globular domains for both α and β subunit has a great advantage of being significantly sensitive to histidine-tagged proteins (McGregor et al., 2008; Liu et al., 2010; Schirmer et al., 1985, 1986). Meantime, previous modeling studies showed that the longer His tag near N-terminus did not significantly interfere with trimer assembly and had a great chance to improve the sensitivity by presenting the histidine side chains on the surface of the trimer (Liu et al., 2010; Cai et al., 2001). The fused His_6-tag provides a convenient method to purify the recombinant APC trimer from the cell lysate on a large-scale (Ge et al., 2009; Liu et al., 2009; Sugiura and Inoue, 1999).

In addition, the large-scale fermentation of functional recombinant APC trimer has also been accomplished successfully. After ultrasonic treatment, conventional protocols of purification for APC trimer with His-tag included three steps: immobilized metal-ion affinity chromatography (IMAC) with chelating transition metal ion (Ni^{2+}), Sephadex G25 size-exclusion chromatography and Superdex 200 size-exclusion chromatography. Three columns were utilized for binding the His-tag proteins, desaltification and obtaining target protein with exact molecular weight, respectively. However, there are several problems in conventional methods. Thus, there is an urgent need to develop efficient methods for purifying the APC trimer.

The first step of separation is the most important to the recombinant APC trimer yield, which is based on the interaction between histidine side chain and Ni^{2+}. But recombinant APC trimer can be disassembled into monomers following an imidazole gradient elution, because of monomer-promoting function of imidazole (Liu et al., 2010; Belew and Porath, 1990). Furthermore, electrostatic interactions including both polar and hydrophobic interactions are responsible for the assembly of monomer and trimer, and the hydrogen bonds which are the strongest noncovalent forces in biological system through functional groups such as carbonyl, amide, or aromatic residues, may play an important role as reported earlier (MacColl et al., 2003; McGregor et al., 2008; McConnell et al., 2010). So, several factors may influence the purification efficiency, among which the most important ones are: imidazole concentration, pH of potassium phosphate and NaCl concentration. Combination effects of the varied factors have not been thoroughly studied. For seeking optima and identifying the combination effect of the individual variables in elution, response surface methodology (RSM) was performed previously (Lee and Gilmore, 2006). Traditional "one-factor at a time" method used to optimize a multivariable system is time-consuming and often missing alternative effects among different components (Bandaru et al., 2006). Therefore, we examined the interactive influences collectively between the three parameters (imidazole concentration, pH of potassium phosphate and NaCl concentration) and purity ratio of APC trimer, using Box-Behnken design by responding surface methodology (RSM) to maximize the trimerization of bAPC trimer (Box and Behnken, 1960; Ragonese et al., 2002; Box and Wilson, 1951). The second step, using size-exclusion chromatography for removal of imidazole is time consuming, low protein recovery, high cost and not adequate to large scale purification (Su et al., 2010). Therefore, replacing the Sephadex G25 size-exclusion chromatography with centrifugal filter device will help in solving this problem, which is speediness, lower cost, simplicity and fitting for large-scale purification.

It is widely accepted that APC monomers and trimers have distinctively different spectral characteristics because of the PCBs in different microenvironments (MacColl et al., 2003). Monomers exhibit a maximum absorption peak at 615 nm, and trimers exhibit absorption maximum at 650 nm with shoulder at around 620 nm (MacColl, 2004). The significant red-shift indicated the trimerization process, and it could provide an easy method for determination of trimerization ratio (MacColl, 2004; MacColl et al., 2003; Liu et al., 2010). In this case, the main peak of 620 nm was observed because of uncompleted trimerization (MacColl et al., 2003; Liu et al., 2010). In order to detect the trimerization ratio of recombinant APC trimer, the $A_{650\ nm}/A_{620\ nm}$ ratio was performed previously (MacColl, 2004; MacColl et al., 2003; Liu et al.,

2010). The aim of the present study was to provide an optimized method, which included the optimized elution buffer in immobilized metal-ion affinity chromatography and centrifugal filter device, for obtaining higher trimerization ratio of recombinant APC trimer. Following additional Superdex 200 size-exclusion chromatography step, the purification of recombinant APC trimer can be completed efficiently. In addition, we firstly report the method for optimization of purification protocol of Histag trimer using response surface methodology.

2. Materials and methods

2.1. Recombinant APC trimer over expression

For preparing the bioengineer APC trimer, the identical strain was conducted according to the previous description, with slightly modification (Liu et al., 2010). The expression vectors of pCDFDeut-1 (spectinomycin resistance) and pRSFDeut-1 (kanamycin resistance) were supplied by Novagen Inc. All materials in this study were from Sigma–Aldrich. Fig. 1A shows the predicted amino acid sequences of apoprotein α subunit and apoprotein β subunit. We tagged six N-terminus polyhistidine on α subunit and β subunit, both of which were amplified from the cyanobacteria *Synechocystis* sp. PCC 6803 by designed PCR primers. In this study, other four genes (*hox1*, *pcyA*, *cpcS-1* and *cpcU*) were also from *Synechocystis* sp. PCC 6803. The bioengineer *E. coli* was cultured at 37 °C in LB medium with 50 mg/L spectinomycin and 50 mg/L kanamycin to 0.4–0.6 $A_{600\ nm}$ value. After adding IPTG to a final concentration of 0.5 mM, expression was induced for 14 h at 28 °C. Cells of approximately 100 g were obtained by centrifugation (7000×g, 30 min) at 4 °C (Fig. 1B).

2.2. Isolation of recombinant APC trimer by IMAC and centrifugal filter device

Cell paste of approximately 100 g was suspended in 1000 mL of binding buffer A1 (20 mM sodium phosphate, 500 mM NaCl, and 20 mM imidazole, pH 7.4) before sonication. After centrifugation (10,000×g, 30 min), the supernatant of sonicated harvest passed through a 0.45 μm filter. A series of equal amounts of filtered supernatant (50 mL) was loaded into 5 mL HisTrap HP chromatography (GE Healthcare Bio-Sciences, USA) at 1 mL/min, using an AKTA fast-performance liquid chromatography system (GE Healthcare Bio-Sciences, USA). Before loading supernatant, the HisTrap HP column was equilibrated to 4 °C with buffer A1. HisTrap HP columns were eluted with 25 mL binding buffer A1 to remove unbound proteins, and then most bound contaminants were eluted by washing with 25 mL buffer A2 (20 mM sodium phosphate, 500 mM NaCl, and 50 mM imidazole, varieties of pH following elution buffer A3) at 1 mL/min. The recombinant APC trimers were finally eluted with a flow rate of 1 mL/min, using varieties of elution buffer A3 to optimize imidazole concentration, pH of potassium phosphate and NaCl concentration. Each eluted fraction at the main peak was collected as target protein. The fractions containing Histag proteins were filled to centrifugal filter device (Millipore Amicon-Ultra-15, USA), in which every unit contained 15 mL sample, with centrifugation 5000×g, 20 min) at 4 °C. Every sample was concentrated to 1 mL and removed the imidazole, and then 14 mL potassium phosphate (50 mM, pH 7.0) was added to the tube with centrifugation (5000×g, 20 min) at 4 °C. Subsequently, above processes of dilution were repeated three times. After dilutions, the final fractions were investigated by absorbance spectra, fluorescence emission spectrum and SDS-PAGE.

2.3. Optimization

A model of 3^3 Box-Behnken design was utilized as an optimization of trimerization ratio within the experimental range (Box and Behnken, 1960; Ragonese et al., 2002). As shown in Tables 1 and 2, pH of potassium phosphate (X_1), NaCl concentration (X_2), and imidazole concentration (X_3) was used as three independent input variables, while the trimerization ratio (Y_1) was chosen as the output variable. Totally, 15 experiments were conducted and the second-order polynomials (Eq. (1)) were calculated to estimate the dependent variable response with SAS (version 8.0):

$$Y_1 = A_0 + A_1X_1 + A_2X_2 + A_3X_3 + A_{12}X_1X_2 + A_{13}X_1X_3 + A_{23}X_2X_3 + A_{11}X_1^2 + A_{22}X_2^2 + A_{33}X_3^2 \quad (1)$$

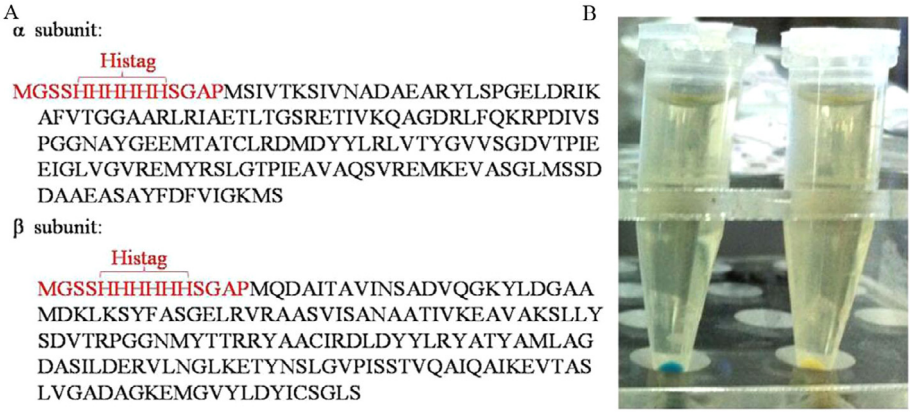

Figure 1 (A) Amino acid sequences and Cell paste of recombinant APC trimer with His tag (red). (B) Protein expression strain (left) and blank control (right).

Table 1 Independent variables in the experimental plan.

Variables	Coded values		
	−1	0	1
pH of potassium phosphate	7	7.5	8
NaCl concentration (mM)	400	500	600
Imidazole concentration (mM)	200	300	400

Table 2 Box-Behnken experimental design with three independent variables.

Run No.	X_1	X_2	X_3	Y_1
1	7(−1)	400(−1)	300(0)	0.852
2	7(−1)	600(1)	300(0)	0.683
3	8(1)	400(−1)	300(0)	0.643
4	8(1)	600(1)	300(0)	0.571
5	7.5(0)	400(−1)	200(−1)	0.756
6	7.5(0)	400(−1)	400(1)	0.780
7	7.5(0)	600(1)	200(−1)	0.706
8	7.5(0)	600(1)	400(1)	0.803
9	7(−1)	500(0)	200(−1)	0.866
10	7(1)	500(0)	200(−1)	0.801
11	7(−1)	500(0)	400(1)	0.871
12	8(1)	500(0)	400(1)	0.864
13	7.5(0)	500(0)	300(0)	0.985
14	7.5(0)	500(0)	300(0)	0.969
15	7.5(0)	500(0)	300(0)	0.993

where X_1, X_2, X_3 are the independent variables, A_0 is the offset term, A_1, A_2, A_3 are the linear coefficients, A_{12}, A_{13}, A_{23} are the interaction terms, A_{11}, A_{22}, A_{33} are the quadratic coefficients and Y_1 is the anticipated response.

2.4. Absorbance and fluorescence spectrometry

Absorbance spectra were measured using a computer-controlled spectrophotometer (Thermo Nanodrop 2000c, USA). The fluorescence emission spectrum were obtained by FluoroMax-4 fluorescence spectrophotometer (HORIBA Jobin Yvon) using 600 nm as excitation wavelength, 620 nm to 750 nm as emission wavelength range and 5 nm as emission slit width.

2.5. SDS-PAGE and Zn^{2+}-UV fluorography

Denatured samples were separated by 15% SDS polyacrylamide gel electrophoresis. After electrophoresis, the protein bands were analyzed by UV-fluorography subsequent to soaking gel in 20 mM zinc sulfate with 10 min. After then, the gels were stained with Coomassie blue R-250.

3. Results

3.1. Optimization of formulation

Fifteen experiments were accomplished using different variables combinations according to the central composite design. Eq. (2) was obtained using Eq. (1) to fit the empirical evidence of trimerization ratio (Y_1) with pH of potassium phosphate (X_1), concentration of Na^+ (X_2), and concentration of imidazole (X_3).

$$Y_1 = 0.982333 + 0.049125X_1 + 0.0335X_2 + 0.023625X_3 - 0.102X_1X_2 - 0.02425X_1X_3 + 0.0145X_2X_3 - 0.192167X_1^2 + 0.01825X_2^2 - 0.028917X_3^2 \quad (2)$$

The summary of variance of the predicted results of Y_1 and the regression model by Eq. (2) is shown in Table 3. The fitness of the model could be checked against different criteria. In this case, R^2 is 93.49% which indicated that 93.49% of the total variations in response could be explained using this model for coefficient of determination. In addition, the F-value of the model at 6.834309 indicated that the model was reasonable. The value of "Probe > F" less than 0.05 suggests that the model terms are fitting. Fig. 2 represents three-dimensional contour plots for the optimization of formulation. In the design bounds, each plot of response surface had a significant top point and the corresponding contour plot had a significant peak point, which clearly indicated that the highest point of Y_1 could be involved in the design bounds.

RSM is often applied in engineering and manufacturing for several important advantages. For example, researchers could easily use considerable less experimental efforts with determining the impact of a factor, identifying of factors, finding optima, offering well precision and facilitating system. In this experiment, using Box-Behnken experimental design, we

Table 3 ANOVA for the entire quadratic model.

Factors	Degrees of freedom	Sum of squares	Mean square	F-value	Probe > F
Model	9	0.202705	0.022523	7.973006	0.017089
X_1	1	0.019306	0.019306	6.834309	0.047426
X_2	1	0.008978	0.008978	3.178184	0.134718
X_3	1	0.004465	0.004465	1.58064	0.264197
X_1^2	1	0.039108	0.039108	13.84423	0.013701
X_1X_2	1	0.002352	0.002352	0.832689	0.403349
X_1X_3	1	0.000841	0.000841	0.297711	0.608771
X_2^2	1	0.13635	0.13635	48.26735	0.000949
X_2X_3	1	0.001332	0.001332	0.471612	0.522792
X_3^2	1	0.003087	0.003087	1.092934	0.343706
Lack of fit	3	0.013826	0.004609	30.86105	0.03155
Pure Error	2	0.000299	0.000149		
Total	14	0.21683			

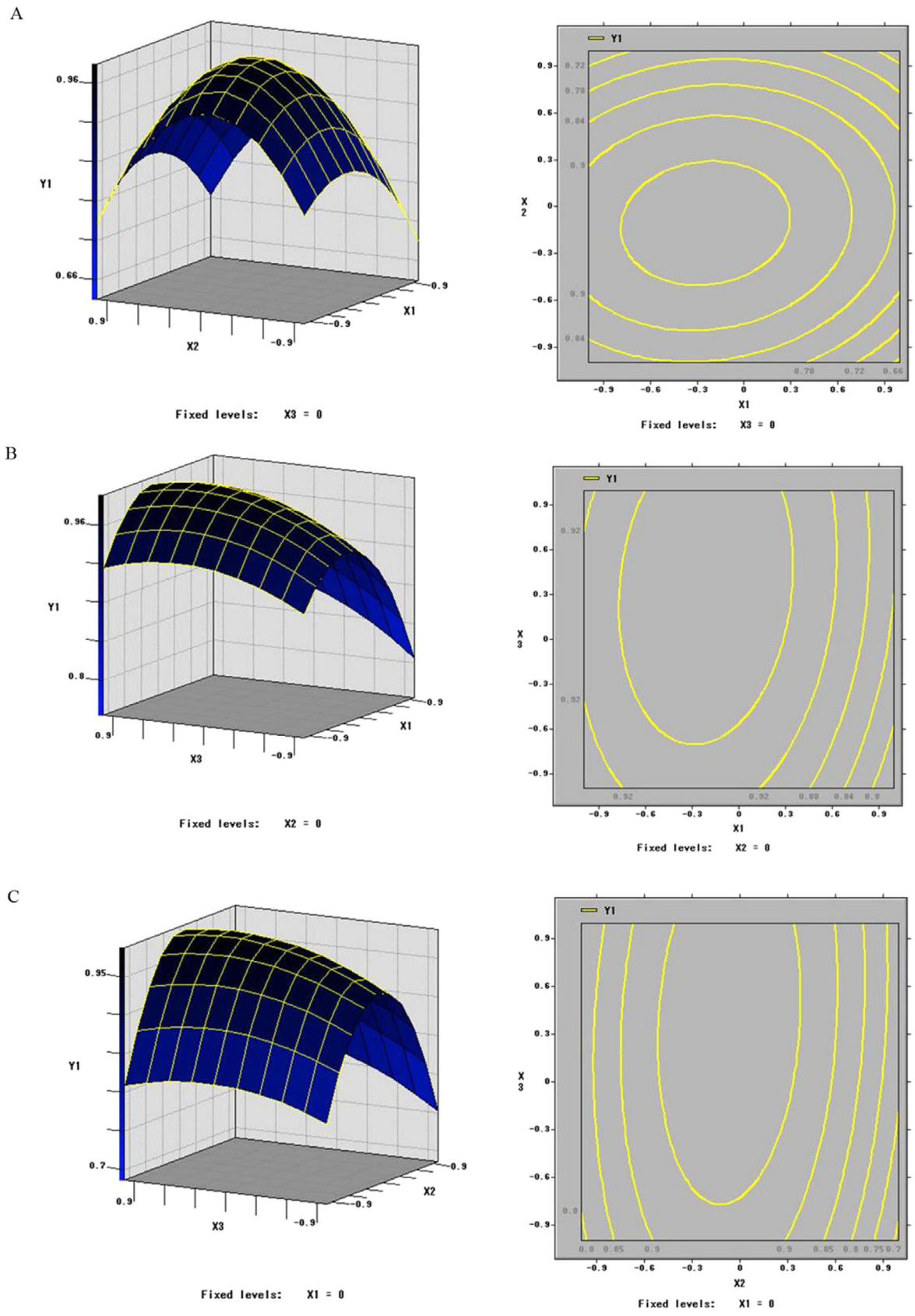

Figure 2 Three dimensional contour plots for the maximum Y_1. RSM plots were generated using the data shown in Table 3. Inputs were the 15 experimental runs which carried out under the conditions established by the Box-Behnken experimental design. (A) X_1 vs. X_2 on trimerization ratio (B) X_1 vs. X_3 on trimerization ratio (C) X_2 vs. X_3 on trimerization ratio.

determined the optima near the central pH of potassium phosphate, NaCl concentration and imidazole concentration. The optimum formulation obtained was pH of potassium phosphate at 7.38, NaCl concentration at 491.4 mM and imidazole concentration at 332.5 mM, respectively. A predicted maximum trimerization ratio of approximate $A_{650\ nm}/A_{620\ nm}$ at 0.993 was obtained at these optimum parameters. We verified the predicted maximum in a trial run, in excellent agreement with predicted value. The trimerization ratio of $A_{650\ nm}/A_{620\ nm}$ was 1.024 and the relative error was 3% with the predicted value. Absorbance spectrometry of the optimization experiments is shown in Fig. 3, which shows the desired trimerization ratio of bAPC trimer, compared with the main absorbent peak at 650 nm with that at 620 nm from Liu' s previous report in 2009.

3.2. Fluorescence emission spectra and gel electrophoresis examination

After purification following these optimum parameters, a serial of further examinations were carried out. Fig. 4 exhibits fluorescence spectra with emission maximum at 660 nm with shoulder at around 640 nm, which demonstrated the formation of recombinant APC trimer complexes, consistent with the previous reports (MacColl, 2004; MacColl et al., 2003; Liu et al., 2010). Moreover, the results of APC trimer purification were confirmed by Coomassie staining and Zn^{2+}-UV-fluorography of SDS polyacrylamide gel electrophoresis (Fig. 5). The SDS-PAGE images of Fig. 5 reveal that there were two main bands in lane 2 at the expected position, both Coomassie stain and orange fluorescence. The excited fluorescence was visualized under ultraviolet rays, because of the linkages of zinc ion and chromophore (Tooley et al., 2001; Berkelman and Lagarias, 1986). The special fluorescent property was direct proof of the presence of covalently bonded chromophore. As compared to molecular mass standard, two main bands were obtained at 21 kDa and 19 kDa with Coomassie stain, closely matching the theoretical molecular weights of α (band a) and β (band b) subunits with Histag (Liu et al., 2010). In addition, the bands of orange fluorescence

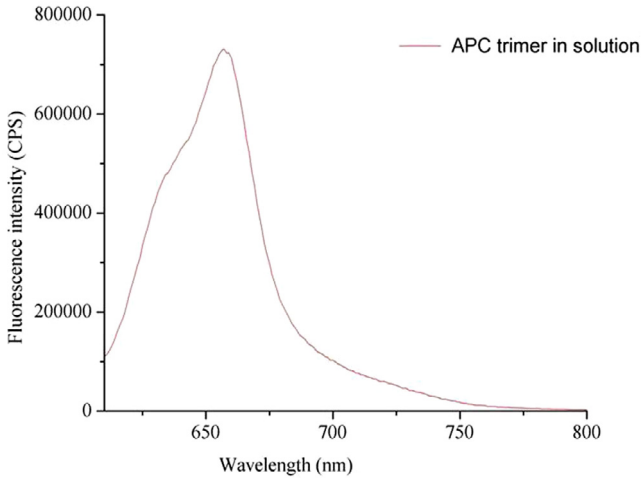

Figure 4 Fluorescence emission spectrum of the bAPC trimer in solution.

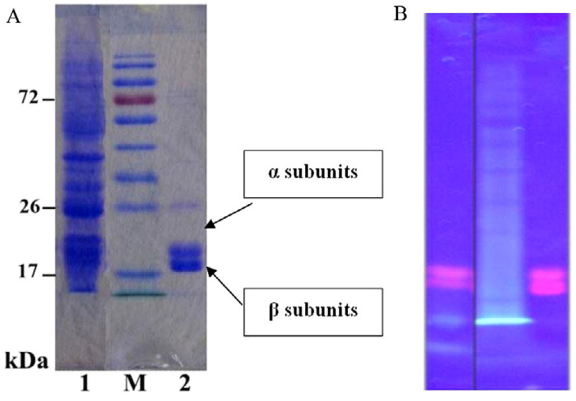

Figure 5 Electrophoresis imaging of bAPC trimer purification. (A) Gels were stained with Coomassie blue R-250. (B) UV-exited fluorescence binding with zinc ions. Line1: background of *E. coli* extract (cell lysate). Line2: APC trimer purification. M: Protein Molecular Weight Marker.

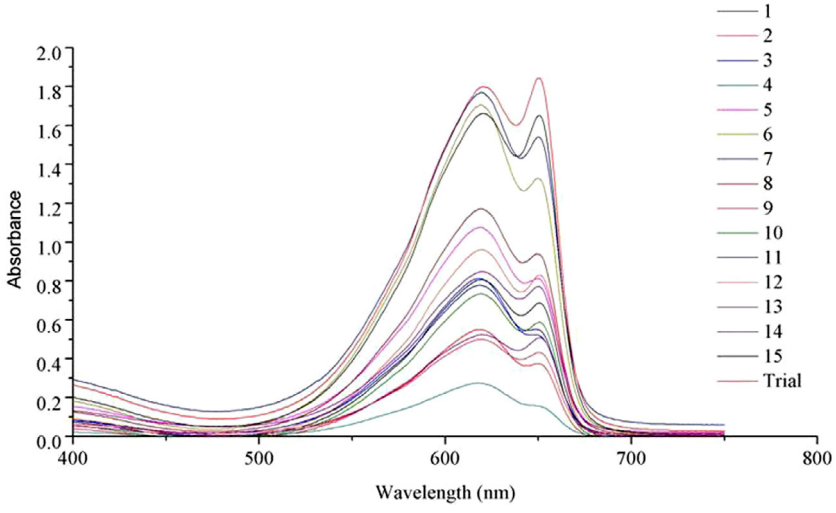

Figure 3 Absorbance spectra of the APC trimer for optimization.

were consistent with the bands of Coomassie stain. Meantime, the same results were observed, comparing to background of *E. coli* extract in lane 1 (cell lysate). Most importantly, the intensity analysis of Coomassie stain showed that the amount of α subunits was equivalent approximately to β subunits, in despite of slight contaminant protein bands.

4. Discussion

As the previous reports, the assembly of an APC monomer is due to the hydrophobic interactions and electrostatic interactions (charge-charge interactions, hydrogen bonds) (McGregor et al., 2008; McConnell et al., 2010; Wiegand et al., 2002). As evidenced by X-ray crystallography, the hydrophobic interactions between α-helices X and Y of same subunit and the globular domain of its partner subunit are prominently responsible for the formation of APC monomer (McGregor et al., 2008). There are also many types of hydrogen bonds in the formation of APC monomer, respectively, hydroxyl-hydroxyl, hydroxyl-carbonyl, amide-carbonyl and amide-hydroxyl. The formation of APC trimer is similar to the above pattern. But the interaction surface between monomers is only proximately 50% of the interaction surface between α and β subunit, hinting the weaker stability of APC trimers than monomers (McGregor et al., 2008; Huang et al., 1987; Kupka and Scheer, 2008). In addition, the hydrogen bonds between polypeptide backbone and water, between polypeptide backbone and polar side chains, between two polar side chains and between polar side chains and water are present in hydrophobic core and near the surface. It is possible that there are more stably internal hydrogen bonds without the competition with water molecules in APC monomers than in APC trimer. Using the native APC as a model, above descriptions provided a reasonable explanation of the phenomenon that bAPC trimers were dissociated into monomer rather than subunits, under the same elution conditions.

bAPC trimer binding was based on the formation of coordination bonds between unoccupied coordination sites of Ni^{2+} ion and histidine tags of the protein surface, which Ni^{2+} ion coordinated six ligands with polyhistidine and chelater in an octahedral complex (Belew and Porath, 1990; Davankov and Semechkin, 1977). Elution was mainly due to competing ligands from imidazole (Sulkowski, 1996a,b). In the meantime, sodium chloride can affect the elution by reducing electrostatic interactions and interactions between chloride ions and Ni^{2+} ion; the increase of pH is associated with an increased competition from hydroxyl ions for coordination sites of Ni^{2+} ions. However, following elution, trimer dissociation could occur as a result of a disruption of hydrogen bonds, which was caused by direct interaction between imidazole and polypeptide backbone contacts. The competition with imidazole nitrogen for hydrogen bond sites of bAPC trimer which located contact surface between monomers might be an explanation of the disruption. Although lower imidazole concentration in elution buffer may reduce the disruption, the elution time is longer than the elution with higher imidazole concentration. A longer elution time may even increase risk of dissociation of bAPC trimer, which is consistent with our results. It may thus be necessary to keep an appropriate imidazole concentration, as our works. Chloride ions, as counter ligand of Ni^{2+}, is usually used for a decrease of nonspecific electrostatic interactions and contribution to the elution efficiency by interactions between chloride ions and Ni^{2+}, but high-ionic-strength might increase the dissociation of bAPC trimer. In addition, protonation of histidine at lower pH under pH 6.0 could be beneficial to an effective desorption, but bAPC trimer is very easy to form monomers due to sensitive to the acid conditions (MacColl, 2004). Moreover, higher pH above pH 8.0 also decreases histidine coordination strength, but there will be a great possible monomerization because of an increased competition from hydroxyl ions for hydrogen bond sites of bAPC trimer which located contact surface between monomers. From the above discussion, it is reasonable that the varied factors are correlative and imidazole concentration play a main role. Intrinsic properties of the bAPC trimer such as stability in neutral pH, natural function in low-ionic-strength aqueous solution, also support our suggestions for the potentially best possible conditions.

In conclusion, this work suggests an optimized protocol to achieve the desired trimerization ratio of bAPC trimer. The method could be served as a new paradigm for the purification protocol of the polymeric form of protein complex with fused histidine peptides and will help in designing the purification protocol of a lager sample on a large column.

Acknowledgments

The authors gratefully thank the financial support provided by the Science Foundation of the Chinese Academy of Sciences (XDA1102040300) and Ocean Public Welfare Scientific Research Project, State Oceanic Administration of China (201205027). This work was also supported by the National Key Technology R&D Program of China (Grant No. 2013BAB01B01) and Scientific Research Foundation of Ludong University (ly2014041). Dr. Hainan Su (Shandong University) is acknowledged for the help with spectra analysis.

References

Adir, N., 2005. Elucidation of the molecular structures of components of the phycobilisome: reconstructing a giant. Photosynth. Res. 85 (1), 15–32.

Adir, N., Dines, M., David, L., Klartag, M., McGregor, A., Melamed-Frank, M., Sendersky, E., Schwarz, R., 2007. Structural aspects of the assembly and disassembly of the Phycobilisome. Photosynth. Res. 91 (2–3). 157-157.

Arteni, A.A., Ajlani, G., Boekema, E.J., 2009. Structural organisation of phycobilisomes from Synechocystis sp strain PCC6803 and their interaction with the membrane. Biochim. Biophys. Acta (BBA)-Bioenergetics 1787 (4), 272–279.

Bandaru, V.V.R., Somalanka, S.R., Mendu, D.R., Madicherla, N.R., Chityala, A., 2006. Optimization of fermentation conditions for the production of ethanol from sago starch by co-immobilized amyloglucosidase and cells of Zymomonas mobilis using response surface methodology. Enzyme Microb. Technol. 38 (1–2), 209–214.

Belew, M., Porath, J., 1990. Immobilized metal ion affinity chromatography. Effect of solute structure, ligand density and salt concentration on the retention of peptides. J. Chromatogr. 516 (2), 333–354.

Berkelman, T.R., Lagarias, J.C., 1986. Visualization of bilin-linked peptides and proteins in polyacrylamide gels. Anal. Biochem. 156 (1), 194–201.

Bermejo, R., Talavera, M., Alvarez-Pez, J., Orte, J.C., 1997. Chromatographic purification of biliproteins from Spirulina platensis

high-performance liquid chromatographic separation of their α and β subunits. J. Chromatogr. A 778 (1–2), 441–450.
Box, G.E.P., Behnken, D.W., 1960. Simplex-sum designs: a class of second order rotatable designs derivable from those of first order. Ann. Math. Stat. 31 (4), 838–864.
Box, G.E.P., Wilson, K.B., 1951. On the experimental attainment of optimum conditions. J. R. Stat. Soc. B-Stat. Methodol. 13 (1), 1–45.
Cai, Y.A., Murphy, J.T., Wedemayer, G.J., Glazer, A.N., 2001. Recombinant phycobiliproteins. Recombinant C-phycocyanins equipped with affinity tags, oligomerization, and biospecific recognition domains. Anal. Biochem. 290 (2), 186–204.
Davankov, V.A., Semechkin, A.V., 1977. Ligand-exchange chromatography. J. Chromatogr. 141 (3), 313–353.
Ge, B., Sun, H., Feng, Y., Yang, J., Qin, S., 2009. Functional biosynthesis of an allophycocyan beta subunit in Escherichia coli. J. Biosci. Bioeng. 107 (3), 246–249.
Huang, C., Berns, D.S., Maccoll, R., 1987. Kinetics of allophycocyanin's trimer-monomer equilibrium. Biochemistry 26 (1), 243–245.
Kupka, M., Scheer, H., 2008. Unfolding of C-phycocyanin followed by loss of non-covalent chromophore-protein interactions 1. Equilibrium experiments. Biochim. Biophys. Acta (BBA)-Bioenergetics 1777 (1), 94–103.
Lee, K.M., Gilmore, D.F., 2006. Statistical experimental design for bioprocess modeling and optimization analysis. Appl. Biochem. Biotechnol. 135 (2), 101–115.
Liu, S., Chen, H., Qin, S., Zhang, W., Guan, X., Lu, Y., 2009. Highly soluble and stable recombinant holo-phycocyanin alpha subunit expressed in Escherichia coli. Biochem. Eng. J. 48 (1), 58–64.
Liu, S., Chen, Y., Lu, Y., Chen, H., Li, F., Qin, S., 2010. Biosynthesis of fluorescent cyanobacterial allophycocyanin trimer in Escherichia coli. Photosynth. Res. 105 (2), 135–142.
Lowe, C.D., 2007. Optimization and Stabilization of Phycobilisomes for use in Applied Phototechnology. University of Tennessee Honors Thesis Projects, http://trace.tennessee.edu/utk_chanhonoproj/1092.
MacColl, R., 2004. Allophycocyanin and energy transfer. Biochim. Biophys. Acta (BBA)-Bioenergetics 1657 (2–3), 73–81.
MacColl, R., Eisele, L.E., Menikh, A., 2003. Allophycocyanin: trimers, monomers, subunits, and homodimers. Biopolymers 72 (5), 352–365.
McConnell, I., Li, G.H., Brudvig, G.W., 2010. Energy conversion in natural and artificial photosynthesis. Chem. Biol. 17 (5), 434–447.
McGregor, A., Klartag, M., David, L., Adir, N., 2008. Allophycocyanin trimer stability and functionality are primarily due to polar enhanced hydrophobicity of the phycocyanobilin binding pocket. J. Mol. Biol. 384 (2), 406–421.
Nelson, N., Yocum, C.F., 2006. Structure and function of photosystems I and II. Annu. Rev. Plant Biol. 57 (57), 521–565.
Ragonese, R., Macka, M., Hughes, J., Petocz, P., 2002. The use of the Box-Behnken experimental design in the optimisation and robustness testing of a capillary electrophoresis method for the analysis of ethambutol hydrochloride in a pharmaceutical formulation. J. Pharmaceut. Biomed. Anal. 27 (6), 995–1007.
Schirmer, T., Bode, W., Huber, R., Sidler, W., Zuber, H., 1985. X-ray crystallographic structure of the light-harvesting biliprotein C-phycocyanin from the thermophilic cyanobacterium Mastigocladus laminosus and its resemblance to globin structures. J. Mol. Biol. 184 (2), 257–277.
Schirmer, T., Huber, R., Schneider, M., Bode, W., Miller, M., Hackert, M.L., 1986. Crystal structure analysis and refinement at 2.5 A of hexameric C-phycocyanin from the cyanobacterium Agmenellum quadruplicatum. The molecular model and its implications for light-harvesting. J. Mol. Biol. 188 (4), 651–676.
Su, H.N., Xie, B.B., Chen, X.L., Wang, J.X., Zhang, X.Y., Zhou, B. C., Zhang, Y.Z., 2010. Efficient separation and purification of allophycocyanin from *Spirulina* (Arthrospira) platensis. J. Appl. Phycol. 22 (1), 65–70.
Sugiura, M., Inoue, Y., 1999. Highly purified thermo-stable oxygen-evolving photosystem II core complex from the thermophilic cyanobacterium *Synechococcus elongatus* having His-tagged CP43. Plant Cell Physiol. 40 (12), 1219–1231.
Sulkowski, E., 1996. Immobilized metal-ion affinity chromatography: imidazole proton pump and chromatographic sequelae. II. Chromatographic sequelae. J. Mol. Recognit. 9 (5–6), 494–498.
Sulkowski, E., 1996a. Immobilized metal-ion affinity chromatography: imidazole proton pump and chromatographic sequelae. I. Proton pump. J. Mol. Recognit. 9 (5–6), 389–393.
Tooley, A.J., Cai, Y.P.A., Glazer, A.N., 2001. Biosynthesis of a fluorescent cyanobacterial C-phycocyaninholo-alpha subunit in a heterologous host. Proc. Natl. Acad. Sci. U.S.A. 98 (19), 10560–10565.
Wiegand, G., Parbel, A., Seifert, M.H., Holak, T.A., Reuter, W., 2002. Purification, crystallization, NMR spectroscopy and biochemical analyses of alpha-phycoerythrocyanin peptides. Eur. J. Biochem. 269 (20), 5046–5055.